ISSN 1330-3651 (Print), ISSN 1848-6339 (Online) https://doi.org/10.17559/TV-20230128000280
Original scientific paper

Reissner-Mindlin Based Isogeometric Finite Element Formulation for Piezoelectric Active Laminated Shells

Predrag MILIĆ, Dragan MARINKOVIĆ*, Sandra KLINGE, Žarko ĆOJBAŠIĆ

Abstract: The paper deals with the isogeometric analysis (IGA) of active composite laminates with piezoelectric layers. IGA is a special formulation of the finite element method (FEM) that aims at seamless integration of geometric and finite element modelling. NURBS basis functions are employed to develop isogeometric shell formulation based on the Reissner-Mindlin kinematics. Piezolayers characterized by electro-mechanical coupled field effects enable active behavior of the considered structures. The electric field acts across the thickness of the piezolayers and is coupled to the in-plane strains. In addition to a number of advantages that NURBS modelling provides, defining the surface normal vector at the points of the control polygon, which are generally not located on the surface, creates certain difficulties. A method of determining the surface normal vectors at the points of the control polygon based on the Greville's points is discussed. In order to demonstrate the applicability of the developed formulation, a benchmark case is computed and the results are compared with those obtained by means of classical FEM formulation, which are available in the literature.

Keywords: grevill points; isogeometric analysis; laminated Reissner-Mindlin shell; piezolayer

1 INTRODUCTION

The progress of science and technology led to the emergence of modern structures, which are not only lightweight, but also kind of 'smart'. The lightweight property is attributed to advanced materials, primarily fiber-reinforced composites, while the structure 'smartness' is due to the so-called active materials like piezoelectric materials [1, 2], shape memory alloys [3], etc. These new materials enabled a dramatic change in the behavior of the structures from conventional passive ones to actively controlled structures, which include capabilities such as self-sensing, signal processing, and control by means of actuation [4]. Smart structures are used in various fields of engineering: aeronautics and space engineering [5], energy harvesting [6, 7], medical applications [8], robotics [9], etc. Particularly lightweight structures benefit from this new design approach in order to reduce the mass of thin-walled structures, the thickness is often reduced to the limits of unwanted deformation, noise and vibrations, which calls for the control of their dynamic behavior [10].

The focus of this paper is on modelling thin-walled active structures with embedded piezoelectric layers, which offer both sensing and actuating options by means of electro-mechanical coupling. To investigate the kinematics of laminated shell structures, various 2D theories can be used [11]. Some developments were based on the classical laminate theory [12]. However, the first-order shear deformation theory was much more employed due to its better suitability for laminated structures, which are prone to transverse shear effects [13, 14]. Higher-order shear deformation theories were applied as well [15, 16], however the numerical effort with these theories is nearly the same as with the full 3D approach, which is disadvantageous. Novel developments were focused on geometrically nonlinear formulations [17, 18].

Isogeometric analysis, proposed by Hughes et al. [19], aims to close the gap between the CAD (or actual) geometry and the geometry used upon finite element (FE) discretization. There are several different isogeometric shell formulations: Kirchhoff-Love [20-22], Mindlin-Reissner [23], higher-order kinematics [24]. Models of isogeometric laminated composite shells have also been developed [25, 26].

The accuracy of the results of the isogeometric analysis of the shell largely depends on the precisely determined normal vectors at the points of the control polygon. Considering that they do not have a unique projection on the middle plane of the shell, several researchers have investigated this problem [27, 28].

Upon providing the motivation to work on this topic and a short overview of different directions of development in the field of active piezoelectric laminates, the rest of the manuscript is organized as follows. The next section provides basics related to B-splines and NURBS basic functions. This is followed by the procedure of finite element mesh refinement and the determination of the director vectors normal to the reference surface at control points, both within the framework of isogeometric FE formulation. Upon defining the displacement field, the mechanical and piezoelectric constitutive equations are used to define the finite element matrices for the coupled field problem. The derived FE formulation is applied to a benchmark case in order to demonstrate the development. Finally, the concluding remarks of the study are given.

2 B-SPLINE AND NURBS BASIC FUNCTIONS

In this work, the geometry of the FE model is based on NURBS surfaces (NURBS-Non-Uniform Rational B-Splines). The model properties are influenced by this fact and, therefore, the basis spline (B-spline), NURBS functions, as well as curves and surfaces based on them are addressed below.

NURBS has a clear advantage compared to a B-spline related to the possibility of accurate descriptions of quite complex geometric shapes. NURBS are actually built by using B-splines as basic functions.

Cox-De Boor's recursive formula [29] is used to define a B-spline of the order p based on a knot vector $\Xi = [\xi_0, \xi_1, ..., \xi_{n+p+1}]$. For $p = 0$, the basic functions read:

$$N_{i,0}(\xi) = \begin{cases} 1 & \xi_i \le \xi < \xi_{i+1} \\ 0 & \text{otherwise} \end{cases} \tag{1}$$

Higher order basic functions are defined in this manner:

$$N_{i,p}(\xi)=\frac{\xi-\xi_i}{\xi_{i+p}-\xi_i}N_{i,p-1}(\xi)+\frac{\xi_{i+p+1}-\xi}{\xi_{i+p+1}-\xi_{i+1}}N_{i+1,p-1}(\xi) \quad (2)$$

The knot vector is given as a set of parametric coordinates ξ_i in a non-decreasing order. The function order, p, and knot multiplicity determine the continuity of basis functions. If the knot multiplicity is k, the continuity is C^{p-k}. Further characteristics of the basic functions are: $N_{i,0}(\xi)$ is a stepped function equal to zero for all ξ except for a half open interval $\xi\in[\xi_i, \xi_{i+1})$; $N_{i,p}(\xi)$ is defined as a linear combination of two functions of degree $(p-1)$; a basic function of order p has a value different from zero only in the semi-interval $\xi\in[\xi_i, \xi_{i+p+1})$; sum of all basic functions of the order p at a point ξ is equal to 1 (partition of unity); the functions are non-negative and linearly independent.

A p-order NURBS curve is represented as a rational function based B-spline basic functions as given below [29, 30]:

$$C(\xi)=\frac{\sum_{i=0}^{n}N_{i,p}(\xi)w_iP_i}{\sum_{i=0}^{n}N_{i,p}(\xi)w_i}=\sum_{i=0}^{n}R_{i,p}(\xi)P_i,\ a\le\xi\le b \quad (3)$$

where P_i are the control points forming a control polygon, w_i are the weights, $\{N_{i,p}(\xi)\}$ are the B-spline basic functions of the order p defined on the non-uniform knot vector $\Xi=\{a, ..., a, \xi_{p+1}, ..., \xi_{m-p-1}, b, ..., b\}$, and $R_{i,p}$ are the p-order basic rational functions of the NURBS.

The knot vector is usually normalized, so that $a=0$ and $b=1$. The order of spline defines how many times the elements a and b are repeated in the knot vector. In this way, the discontinuity is realized at the ends of the spline. A NURBS surface of the order p in the ξ direction and order q in the η direction is given as:

$$S(\xi,\eta)=\frac{\sum_{i=0}^{n}\sum_{j=0}^{m}N_{i,p}(\xi)N_{j,q}(\eta)w_{ij}P_{ij}}{\sum_{k=0}^{n}\sum_{l=0}^{m}N_{k,p}(\xi)N_{l,q}(\eta)w_{k,l}}\ 0\le\xi,\eta\le1 \quad (4)$$

Introducing the basic rational function:

$$R_{ij}(\xi,\eta)=\frac{N_{i,p}(\xi)N_{j,q}(\eta)w_{ij}}{\sum_{k=0}^{n}\sum_{l=0}^{m}N_{k,p}(\xi)N_{l,q}(\eta)w_{kl}}\ 0\le\xi,\eta\le1 \quad (5)$$

the equation for the surface reads:

$$S(\xi,\eta)=\sum_{i=0}^{n}\sum_{j=0}^{m}R_{ij}(\xi,\eta)P_{ij},\ 0\le\xi,\eta\le1 \quad (6)$$

3 FINITE ELEMENT MESH AND DIRECTOR VECTORS AT CONTROL POINTS

An example of a NURBS surface (patch) defined as per Eq. (5) is shown in Fig. 1. The NURBS surface is defined by points of control polygon in the physical space, index vectors in the index space and by degrees of the basic functions. The boundaries of element surfaces are defined in the parameter space (Fig. 2). Upon mapping into the physical space (Fig. 1), the elements of the NURBS surface can be observed. Each element-surface is defined on half open intervals $\xi\in[\xi_i, \xi_{i+1})$; and $\eta\in[\eta_j, \eta_{j+1})$. This is the initial mesh of elements.

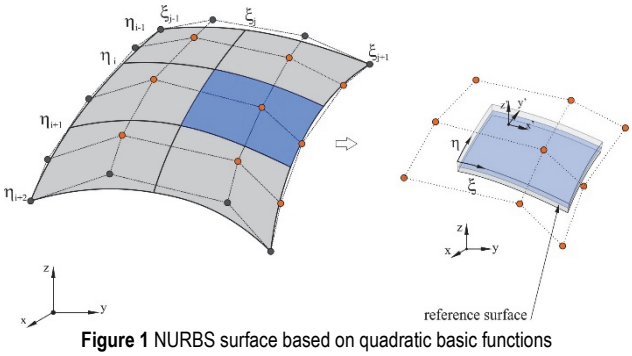

Figure 1 NURBS surface based on quadratic basic functions

The geometry of the element reference surface (as part of the patch) is determined by the mesh of the control polygon points with the corresponding weight coefficients and corresponding NURBS basis functions $R_{ij}(\xi,\eta)$ on the half open intervals $\xi\in[\xi_i, \xi_{i+1})$ and $\eta\in[\eta_j, \eta_{j+1})$. Other NURBS basic functions of the patch outside the half open interval have a zero value, and therefore the points of the control polygon corresponding to them have no influence on this part of geometry. For the sake of simplicity, all control points that affect the geometry of element as well as their corresponding basic functions will be numbered from 1 to n_{en}, where $n_{en}=(p+1)(q+1)$. Fig. 1 shows a patch with the element and its corresponding control polygon points marked.

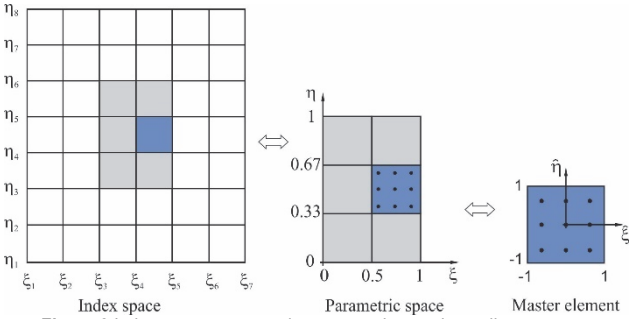

Figure 2 Index space, parametric space and natural coordinate system

Isogeometric analysis closes the gap between the CAD geometry obtained from a CAD modeller and the finite element geometry. The initial number of elements along each direction is determined for the initial mesh by the following equation and is clearly visible in the parameter space:

$$n_e=(n-p)(m-q) \quad (7)$$

where m and n are the number of basic functions (i.e. points of control polygon) along the ξ and η directions, and p and k are the degrees of the basic functions in the ξ and η directions.

The initial mesh can be changed with the techniques of knot insertion into the knot vectors (h-refinement), increasing the degree of basic functions (p-refinement) and increasing the degree of basic functions with the subsequent insertion of a new knot into the knot vectors (k-refinement). With the last mentioned technique, the degree of the basic functions and the density of the mesh are increased with the aim of increasing the degree of continuity at the elements boundaries.

For the formulation of the shell isogeometric finite element type, we need four coordinate systems:
- the global Cartesian coordinate system (x, y, z),
- the natural coordinate system (r, s, t) - an orthonormal system with $-1 < r, s, t < +1$,
- the local Cartesian coordinate system (x', y', z'),
- the curvilinear coordinate system (ξ, η, ζ).

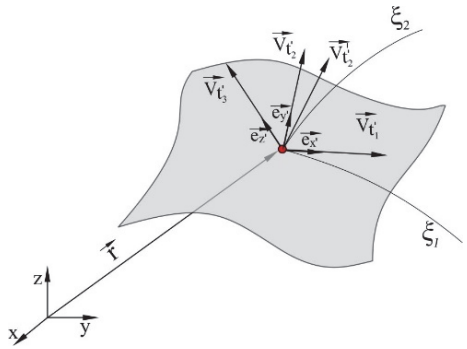

Figure 3 Defining the coordinate system at a point on the reference surface

The tangent plane at a point on the surface is defined by vectors $\vec{V}_{t_1'}$ and $\vec{V}_{t_2'}$. They are determined as derivatives of the position vector r by the variables ξ and η.

$$\vec{V}_{t_1}' = \frac{\partial \vec{r}}{\partial \xi} = \sum_{k=1}^{n_{en}} \frac{\partial R_k(\xi, \eta)}{\partial \xi} P_k$$
$$\vec{V}_{t_2}' = \frac{\partial \vec{r}}{\partial \eta} = \sum_{k=1}^{n_{en}} \frac{\partial R_k(\xi, \eta)}{\partial \eta} P_k \tag{8}$$

where $R_k(\xi, \eta)$ and P_k are the basic functions and the points of the control polygon on the element reference surface on which the observed point is located. The obtained vectors, $\vec{V}t_1'$ and $\vec{V}t_2'$, are not generally perpendicular to each other. It is necessary to form an orthogonal coordinate system. The vector product of the previous two vectors gives a vector normal to the tangent plane.

$$\vec{V}_{z'} = \vec{V}_{t_1'} \times \vec{V}_{t_2}' \tag{9}$$

An orthonormalized coordinate system was formed by Eq. (11):

$$\vec{V}_{t_2'} = \vec{V}_{z'} \times \vec{V}_{t_1'} \tag{10}$$

$$\vec{e}_{x''} = \frac{\vec{V}_{t_1'}}{\left|\vec{V}_{t_1'}\right|} = \begin{Bmatrix} l_1'' \\ m_1'' \\ n_1'' \end{Bmatrix}, \vec{e}_{y''} = \frac{\vec{V}_{t_2'}}{\left|\vec{V}_{t_2'}\right|} = \begin{Bmatrix} l_2'' \\ m_2'' \\ n_2'' \end{Bmatrix}, \vec{e}_{z''} = \frac{\vec{V}_{z'}}{\left|\vec{V}_{z'}\right|} = \begin{Bmatrix} l_3'' \\ m_3'' \\ n_3'' \end{Bmatrix} \tag{11}$$

In order to form a finite element model with a shell element type using the isogeometric approach, it is necessary to determine the vectors normal to the reference surface at the points of the control polygon. In the isogeometric finite element method, most of the control polygon points do not lie on the reference surface, in contrast to the classical finite element method where the nodes are located on the reference surface. In addition, they do not have a unique projection on the reference surface. To determine the vector normal to the reference surface for a certain point of the control polygon, we can find several methods in the literature:
- basis systems obtained by closest point projection,
- calculation of exact basis systems,
- determination of normal vectors in Greville points.

The first method of determining the base system is based on determining the shortest distance between the point of the control polygon and the reference surface. In general, it is not possible to obtain a solution in closed form for this problem. The iterative Newton-Raphson method is most commonly used to solve it. Once the projection point is determined, the orthonormalized coordinate system can be determined according to the previous procedure.

The second method for the exact basis systems calculation uses the fact that, for each element, the normal vectors to the reference surface can be determined at the integration points in two ways. First, the vector normal to the reference surface at the integration point can be determined through the derivative of the position vector with the respect to the variable ξ or η (as shown earlier) and, second, by interpolating over the normal vector at the points of the control polygon (which are currently unknown). It follows that a system of $(p + 1)(q + 1)$ equations has to be formed for each component of all element control points. Also in this case the minimum number of integration points is $(p + 1)(k + 1)$. By increasing the degree of the basic functions, the calculation of the normal vector of the point of the control polygon to the reference surface becomes more difficult. For example, for the degree of basic functions 4, the number of points of the control polygon that is active per element is 25. The minimum number of integration points (to solve the system of equations for the element) per direction is 5, and the total number of equations would be 75 for all three components of the normal vector. In addition, in this way it is necessary to determine one more component of the basic system. If the model is more complex, i.e. with more elements, the problem becomes more demanding to solve.

The third method, which is used here, is based on the determination of the control polygon normal vectors to the reference surface using the Greville points. Greville points, or abscissas, have one-to-one correspondence with the control polygon points. Greville points are defined in the parametric space as follows [31]:

$$\xi_m^{\mathrm{GP}} = \frac{\xi_m + \ldots + \xi_{m+p}}{p}, \ \eta_n^{\mathrm{GP}} = \frac{\eta_n + \ldots + \eta_{n+q}}{q} \tag{12}$$

The number of Greville points corresponds to the number of NURBS basis functions. Hence, it is also equal to the number of control points. Tangent vectors to the reference surface can be formed at Greville's points:

$$\vec{V}_{t_1'}^{GP} = \frac{\partial r}{\partial \xi} = \sum_{k=1}^{n_{en}} \frac{\partial R_k\left(\xi_m^{\mathrm{GP}},\, \eta_n^{\mathrm{GP}}\right)*}{\partial \xi} P_k$$
$$\vec{V}_{t_2'}^{'GP} = \frac{\partial r}{\partial \eta} = \sum_{k=1}^{n_{en}} \frac{\partial R_k\left(\xi_m^{\mathrm{GP}},\, \eta_n^{\mathrm{GP}}\right)}{\partial \eta} P_k \tag{13}$$

In the previous equations, k denotes the number of the element control point and basis function. R_k represents the basic functions of the element that have a value different from zero, P_k represents the points of the control polygon of the corresponding basic functions R_k. The vectors formed at the Greville points lie in the tangent plane to the reference surface at the point with parametric coordinates ξ_m^{GP}, η_n^{GP}. Given that we know the parametric coordinates and normal vectors in the Greville points, we can form a system of equations based on interpolation. By solving the system of equations, we determine the components of vector normal to the reference surface corresponding to the point of control polygon. The point of the control polygon does not have a direct projection on the reference plane. The reason for this is the property of the basic functions of NRUBS, not all of which have the maximum value of 1 (only those on the patch boundaries have the maximum value of 1). The components of the vector normal to the reference surface in the Greville points can be calculated based on the known other two vectors:

$$\vec{V}_3^{\mathrm{GP}} = \frac{\vec{V}_{t_1'}^{'\mathrm{GP}} \times \vec{V}_{t_2'}^{'\mathrm{GP}}}{\left|\vec{V}_{t_1'}^{'\mathrm{GP}} \times \vec{V}_{t_2'}^{'\mathrm{GP}}\right|} \tag{14}$$

On the other hand, the vector components in the Greville points can be represented by the following equation:

$$\vec{V}_{t_n'}^{\mathrm{GP}} = \sum_{k=1}^{n_{en}} R_k\left(\xi_m^{\mathrm{GP}},\, \eta_n^{\mathrm{GP}}\right)\vec{V}_{kl},\; l = 1,\, 2,\, 3 \tag{15}$$

In the previous equation, the vectors V_{kl} at the control points are unknown. In practice, integration is often performed with a reduced number of integration points. In that case, it is not possible to determine the normal vectors, so the determination of normals is done using Greville's points.

4 DIPLACEMENT FIELD

The position of the point on the middle surface can be presented as a function of parametric coordinates:

$$\begin{Bmatrix} x \\ y \\ z \end{Bmatrix} = \sum_{k=1}^{n_{en}} R_k(\xi,\, \eta) \begin{Bmatrix} x_k \\ y_k \\ z_k \end{Bmatrix} \tag{16}$$

The thickness of the shell is assumed to be in the direction normal to the reference surface of the element and can be obtained for any point of the reference surface by means of the interpolation functions and the thickness h_k corresponding to each control point.

$$\begin{Bmatrix} x \\ y \\ z \end{Bmatrix} = \sum_{k=1}^{n_{en}} R_k(\xi,\, \eta) \left\{ \begin{Bmatrix} x_k \\ y_k \\ z_k \end{Bmatrix} + \frac{h_k}{2}\left(t - t_{rk}\right) \begin{Bmatrix} V_{k3x} \\ V_{k3y} \\ V_{k3z} \end{Bmatrix} \right\} \tag{17}$$

where x_k, y_k, z_k are the global coordinates of the control point of element, h_k is the control point correspondent thickness; t_{rk} is the offset of the reference surface from the mid-surface in the natural c.s. of control point k, given as $t_{rk} = 2h_r/h_k$; V_{k3x}, V_{k3y}, V_{k3z} are component of the vector perpendicular to the reference surface at control point P_k (Eq. (15)).

The isogeometric formulation of the element implies the same shape functions for the interpolation of the displacements field as for the CAD and element geometry. Thus, it will be:

$$\begin{Bmatrix} u \\ v \\ w \end{Bmatrix} = \sum_{k=1}^{n_{en}} R_k \left\{ \begin{Bmatrix} u_k \\ v_k \\ w_k \end{Bmatrix} + \begin{Bmatrix} u_k^R \\ v_k^R \\ w_k^R \end{Bmatrix} \right\} \tag{18}$$

where u_k, v_k and w_k represent the nodal displacements along x, y and z axis (global displacements) respectively and $u^{\mathrm{R}}_{\mathrm{k}}$, $v^{\mathrm{R}}_{\mathrm{k}}$ and $w^{\mathrm{R}}_{\mathrm{k}}$ are the relative displacements of the point on the thickness direction line through the control point k with respect to the control point, resulting from the rotation od the line, and of course along x, y and z axis. The displacements u^R_k, v^R_k and w^R_k are to be expressed in terms of the nodal rotations θ_{xk}, θ_{yk} and θ_{zk} (global rotations).

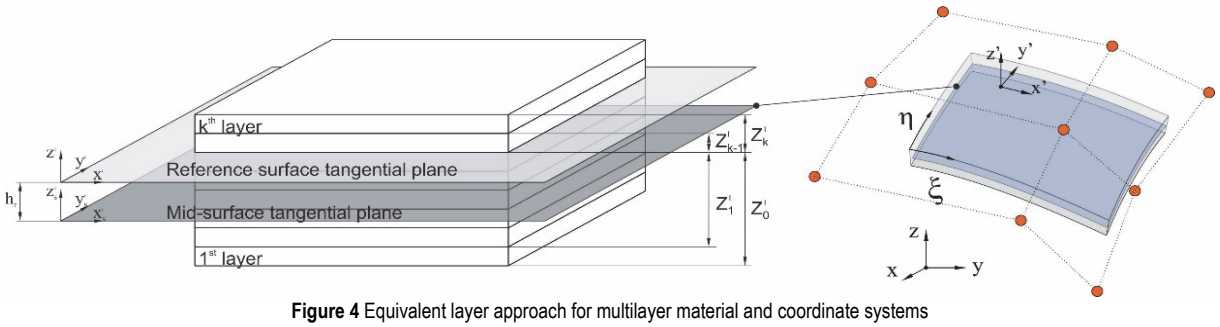

Figure 4 Equivalent layer approach for multilayer material and coordinate systems

In order to do that, the assumption that the thickness direction line remains straight after deformation will be used (Reissner-Mindlin kinematics). Threfore, in the local coordinate system fixed to the control point k, the following relations can be written:

$$\begin{Bmatrix} u_k^R \\ v_k^R \\ w_k^R \end{Bmatrix} = \frac{h_k}{2}\left(t - t_{rk}\right)\left[-\vec{V}_{k2},\ \vec{V}_{kl}\right]\begin{bmatrix} \vec{V}_{kl} \\ \vec{V}_{k2} \end{bmatrix}\begin{Bmatrix} q_{xk} \\ q_{yk} \\ q_{zk} \end{Bmatrix} \tag{19}$$

$$\begin{Bmatrix} q_{x'k} \\ q_{y'k} \end{Bmatrix} = \begin{bmatrix} \vec{V}_{kl} \\ \vec{V}_{k2} \end{bmatrix}\begin{Bmatrix} \theta_{xk} \\ \theta_{yk} \\ \theta_{zk} \end{Bmatrix} \tag{20}$$

where $\theta_{x'k}$ and $\theta_{y'k}$ are the nodal local rotation (about the x' and y' axis) Fig. 5.

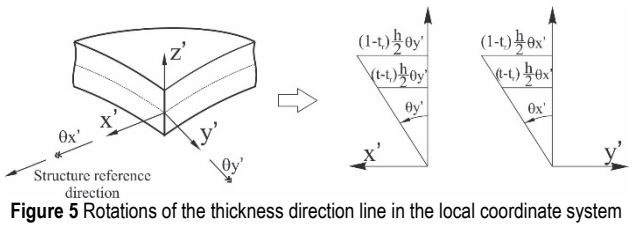

Figure 5 Rotations of the thickness direction line in the local coordinate system

Directionally dependent material properties demand to define the strain field in the local coordinate system. This is usually done so that a distinction is made between the in plane (membrane-flexural) components and the out-of-plane (transverse shear) components:

$$\{\boldsymbol{e}'\} = \begin{Bmatrix} \{\boldsymbol{e}'_{mf}\} \\ -- \\ \{\boldsymbol{e}'_{s}\} \end{Bmatrix} = \begin{Bmatrix} \varepsilon_{x'x'} \\ \varepsilon_{y'y'} \\ \gamma_{x'y'} \\ -- \\ \gamma_{y'z'} \\ \gamma_{x'z'} \end{Bmatrix} = \begin{Bmatrix} \dfrac{\partial u'}{\partial x'} \\ \dfrac{\partial v'}{\partial y'} \\ \dfrac{\partial u'}{\partial y'} + \dfrac{\partial v'}{\partial x'} \\ -- \\ \dfrac{\partial v'}{\partial z'} + \dfrac{\partial w'}{\partial y'} \\ \dfrac{\partial u'}{\partial z'} + \dfrac{\partial w'}{\partial x'} \end{Bmatrix} \tag{21}$$

Derivatives of displacements in the natural coordinate system can be represented by transformation using derivatives of global displacements in the global coordinate system and the transformation matrix:

$$\begin{bmatrix} u'_{,x'} & v'_{,x'} & w'_{,x'} \\ u'_{,y'} & v'_{,y'} & w'_{,y'} \\ u'_{,z'} & v'_{,z'} & w'_{,z'} \end{bmatrix} = \begin{bmatrix} \vec{V}_{kl} \\ \vec{V}_{k2} \\ \vec{V}_{k3} \end{bmatrix}\begin{bmatrix} u_{,x} & v_{,x} & w_{,x} \\ u_{,y} & v_{,y} & w_{,y} \\ u_{,z} & v_{,z} & w_{,z} \end{bmatrix}\left[\vec{V}_{kl} \quad \vec{V}_{k2} \quad \vec{V}_{k3}\right] \tag{22}$$

where, for example, u', $x' = \partial u'/\partial x'$ and u, $x = \partial u/\partial x$.

The transformation of derivatives from the natural to the global coordinate system is done by means of Jacobian inverse matrix:

$$\begin{aligned} [\boldsymbol{J}] &= \begin{bmatrix} x_{,\xi} & y_{,\xi} & z_{,\xi} \\ x_{,\eta} & y_{,\eta} & z_{,\eta} \\ x_{,t} & y_{,t} & z_{,t} \end{bmatrix} = \\ &= \sum_{k=1}^{n_{en}} \begin{bmatrix} \dfrac{\partial N_k}{\partial \xi} x_k & \dfrac{\partial N_k}{\partial \xi} y_k & \dfrac{\partial N_k}{\partial \xi} z_k \\ \dfrac{\partial N_k}{\partial \eta} x_k & \dfrac{\partial N_k}{\partial \eta} y_k & \dfrac{\partial N_k}{\partial \eta} z_k \\ \dfrac{h_k}{2} N_k V_{k3x} & \dfrac{h_k}{2} N_k V_{k3y} & \dfrac{h_k}{2} N_k V_{k3z} \end{bmatrix} \Rightarrow \\ \begin{bmatrix} u_{,x} & v_{,x} & w_{,x} \\ u_{,y} & v_{,y} & w_{,y} \\ u_{,z} & v_{,z} & w_{,z} \end{bmatrix} &= [\boldsymbol{J}]^{-1}\begin{bmatrix} u_{,\xi} & v_{,\xi} & w_{,\xi} \\ u_{,\eta} & v_{,\eta} & w_{,\eta} \\ u_{,t} & v_{,t} & w_{,t} \end{bmatrix} \end{aligned} \tag{23}$$

Using the local displacement derivatives given in Eq. (22), the following form is obtained:

$$\begin{aligned} \{\boldsymbol{e}'\} &= [\boldsymbol{B}_u]\{\boldsymbol{u}\} = \begin{bmatrix} [\boldsymbol{B}_{mf}] \\ -- \\ [\boldsymbol{B}_s] \end{bmatrix}\{\boldsymbol{u}\} = \\ &= \begin{bmatrix} [\boldsymbol{B}_{Tm}] & | & t[\boldsymbol{B}_{Rf}] \\ -- & + & -- \\ [\boldsymbol{B}_{Ts}] & | & [\boldsymbol{B}_{R0s}] + t[\boldsymbol{B}_{R1s}] \end{bmatrix}\begin{Bmatrix} \{\boldsymbol{u}_T\} \\ -- \\ \{\boldsymbol{u}_R\} \end{Bmatrix} \end{aligned} \tag{24}$$

Obviously, the strain–displacement matrix, $[\boldsymbol{B}_u]$ contains the membrane-flexural, $[\boldsymbol{B}_{mf}]$, and transverse shear, $[\boldsymbol{B}_s]$, strain displacement matrices.

5 PIEZOELECTRIC CONSTITUTIVE RELATIONS

Selecting the strain and the electric field as independent variables, the linear piezoelectric constitutive equation in the matrix form is:

$$\begin{aligned} \{\boldsymbol{\sigma}\} &= \left[\boldsymbol{C}^E\right]\{\boldsymbol{\varepsilon}\} - [\boldsymbol{e}]^T\{\boldsymbol{E}\} \\ \{\boldsymbol{D}\} &= [\boldsymbol{e}]\{\boldsymbol{\varepsilon}\} - \left[\boldsymbol{d}^{\varepsilon}\right]\{\boldsymbol{E}\} \end{aligned} \tag{25}$$

where $[\boldsymbol{C}^E]$ is the symmetric material constitutive (Hook's) matrix, $\{\boldsymbol{\sigma}\}$ is the stress vector, $\{\boldsymbol{\varepsilon}\}$ is the strain vector, $[\boldsymbol{e}]$ is the piezoelectric coupling matrix, $\{\boldsymbol{E}\}$ the electric field vector, $\{\boldsymbol{D}\}$ the dielectric displacements vector, $\{\boldsymbol{d}^{\varepsilon}\}$ the vector of dielectric constants (electric displacement to electric field ratio). Stress and strain are second order tensors, but also that for the sake of convenience, they are in the engineering (Voight) notation commonly represented in the form of vectors $\{\boldsymbol{\varepsilon}\}$ and $\{\boldsymbol{\sigma}\}$.

Material properties of commercially available piezoelectric ceramics are transversely isotropic. The above equations can be given together in a developed form, as follows:

$$\begin{Bmatrix} \sigma_{1'1'} \\ \sigma_{2'2'} \\ \sigma_{3'3'} \\ \sigma_{2'3'} \\ \sigma_{1'3'} \\ \sigma_{1'2'} \\ - \\ D_{1'} \\ D_{2'} \\ D_{3'} \end{Bmatrix} = \begin{bmatrix} C_{11} & C_{12} & C_{13} & 0 & 0 & 0 & 0 & 0 & e_{31} \\ C_{12} & C_{11} & C_{13} & 0 & 0 & 0 & 0 & 0 & e_{31} \\ C_{13} & C_{13} & C_{33} & 0 & 0 & 0 & 0 & 0 & e_{31} \\ 0 & 0 & 0 & C_{55} & 0 & 0 & 0 & e_{15} & 0 \\ 0 & 0 & 0 & 0 & C_{55} & 0 & e_{15} & 0 & 0 \\ 0 & 0 & 0 & 0 & 0 & \frac{1}{2}(C_{11}-C_{12}) & 0 & 0 & 0 \\ - & - & - & - & - & - & - & - & - \\ 0 & 0 & 0 & 0 & e_{15} & 0 & -d_{11} & 0 & 0 \\ 0 & 0 & 0 & e_{15} & 0 & 0 & 0 & -d_{11} & 0 \\ e_{31} & e_{31} & e_{33} & 0 & 0 & 0 & 0 & 0 & -d_{33} \end{bmatrix} \begin{Bmatrix} \varepsilon_{1'1'} \\ \varepsilon_{2'2'} \\ \varepsilon_{3'3'} \\ \gamma_{2'3'} \\ \gamma_{1'3'} \\ \gamma_{1'2'} \\ - \\ -E_{1'} \\ -E_{2'} \\ -E_{3'} \end{Bmatrix} \tag{26}$$

The electrodes are placed on the upper and lower surface of the piezolayers. It is assumed that the electric charge is uniformly distributed over the electrodes and, consequently, that the electric field acts in the thickness direction only, so that $E_{1'} = E_{2'} = 0$. The components of the dielectric displacements $D_{1'}$ and $D_{2'}$ are not necessarily equal to zero. However their product with the corresponding components of the electric field ($E_{1'}$ and $E_{2'}$, respectively) in the electric Gibbs energy is zero, which allows the seventh and the eight row and column to be left out of consideration. Hence, the constitutive equation of the piezoelectric layer reads:

$$\begin{Bmatrix} \sigma_{1'1'} \\ \sigma_{2'2'} \\ \sigma_{1'2'} \\ \sigma_{2'3'} \\ \sigma_{1'3'} \\ - \\ D_{3'} \end{Bmatrix} = \begin{bmatrix} Q_{11} & Q_{12} & 0 & 0 & 0 & e'_{31} \\ Q_{12} & Q_{11} & 0 & 0 & 0 & e'_{31} \\ 0 & 0 & Q_{66} & 0 & 0 & 0 \\ 0 & 0 & 0 & Q_{55} & 0 & 0 \\ 0 & 0 & 0 & 0 & Q_{55} & 0 \\ - & - & - & - & - & - \\ e'_{31} & e'_{31} & 0 & 0 & 0 & -d'_{33} \end{bmatrix} \begin{Bmatrix} \varepsilon_{1'1'} \\ \varepsilon_{2'2'} \\ \gamma_{1'2'} \\ \gamma_{2'3'} \\ \gamma_{1'3'} \\ - \\ -E_{3'} \end{Bmatrix} \tag{27}$$

where the following reduced coefficients are introduced:

$$\begin{aligned} &Q_{11} = C_{11} - \frac{C_{13}^2}{C_{33}},\ Q_{12} = C_{12} - \frac{C_{13}^2}{C_{33}}, \\ &Q_{55} = C_{55} - \frac{e_{15}^2}{d_{11}},\ Q_{66} = \frac{1}{2}(C_{11} - C_{12}) \\ &e'_{31} = e_{31} - \frac{C_{13}}{C_{33}} e_{33},\ \ d'_{33} = d_{33} - \frac{e_{33}^2}{C_{33}}, \end{aligned} \tag{28}$$

It is easy to notice that all the shear strain and stress components are decoupled from the rest in Eq. (27). However, this is generally not the case with the in-plane shear components for the considered passive material (fiber-reinforced composite laminates). In order to keep the same approach to obtaining the cross-sectional force and moment resultants as for the passive material, the equations for the transverse shear components will be separated from the in-plane components, thus yielding:

$$\begin{Bmatrix} \sigma_{1'1'} \\ \sigma_{2'2'} \\ \sigma_{1'2'} \\ - \\ D_{3'} \end{Bmatrix} = \begin{bmatrix} Q_{11} & Q_{12} & 0 & e'_{31} \\ Q_{12} & Q_{11} & 0 & e'_{31} \\ 0 & 0 & Q_{66} & 0 \\ - & - & - & - \\ e'_{31} & e'_{31} & 0 & -d'_{33} \end{bmatrix} \begin{Bmatrix} \varepsilon_{1'1'} \\ \varepsilon_{2'2'} \\ \gamma_{1'2'} \\ - \\ -E_{3'} \end{Bmatrix} \tag{29}$$

$$\begin{Bmatrix} \sigma_{2'3'} \\ \sigma_{1'3'} \end{Bmatrix} = kQ_{55} \begin{Bmatrix} \varepsilon_{2'3'} \\ \gamma_{1'3'} \end{Bmatrix} \tag{30}$$

where k is the shear correction factor.

The electric field distribution in the thickness direction of piezoelectric layers should satisfy both, the Maxwell's equations for dielectrics and the element kinematics. The Reissner-Mindlin kinematics would imply linear electric field across the thickness [32]. However, the same investigation [32] shows that the classical assumption of constant electric field over the thickness offers satisfying accuracy for typical, quite thin piezopatches. Hence, the electric field of the kth piezolayer is given by:

$$E_k = \frac{\Delta\Phi_k}{h_k} \tag{31}$$

with $\Delta\Phi_k$ denoting the difference of electric potentials between the electrodes of the kth piezolayer and h_k is the thickness of the piezolayer. This yields a diagonal form of the electric field electric potential matrix:

$$B_\phi = \begin{bmatrix} \ddots & & \\ & \frac{1}{h_k} & \\ & & \ddots \end{bmatrix} \tag{32}$$

6 FINITE ELEMENT DISCRETIZED EQUATIONS

Discretization of a continuum results in a finite element representation. Proceeding in the way characteristic for the finite element method, the generalized displacement field that includes the mechanical displacement field $\{u\}^T = \{u, v, w\}^T$ in the global coordinate system (x, y, z) and the electric potential ϕ of

each piezolayer are related to the corresponding nodal values $\{u\}_i$ and ϕ_i by means of interpolation functions.

In equilibrium, the virtual work of all acting forces in moving through a virtual displacement is zero:

$$\delta W_I + \delta W_E = 0 \tag{33}$$

Assuming a system of conservative forces and that the electric charge of the system is conserved as well (electrically isolated system), the previous equation yields:

$$\begin{aligned}&\int_V \begin{bmatrix} \{\delta\boldsymbol{\varepsilon}\}^{\mathrm{T}}\left[\boldsymbol{C}^{E}\right]\{\boldsymbol{\varepsilon}\} - \{\delta\boldsymbol{\varepsilon}\}^{\mathrm{T}}\left[\boldsymbol{e}\right]^{\mathrm{T}}\{\boldsymbol{E}\} - \{\delta\boldsymbol{E}\}^{\mathrm{T}}\left[\boldsymbol{e}\right]\{\boldsymbol{\varepsilon}\} \\ -\{\delta\boldsymbol{E}\}^{\mathrm{T}}\left[\boldsymbol{d}^{\varepsilon}\right]\{\boldsymbol{E}\} \end{bmatrix} \mathrm{d}V \\ &+\int_V \{\delta\boldsymbol{u}\}^{\mathrm{T}}\{\boldsymbol{F}_{\mathrm{v}}\}\,\mathrm{d}V + \int_{S_1} \{\delta\boldsymbol{u}\}^{\mathrm{T}}\left\{\boldsymbol{F}_{S_1}\right\}\mathrm{d}S_1 \\ &+\sum_{j=1}^{n}\{\delta\boldsymbol{u}\}_j^{\mathrm{T}}\{\boldsymbol{F}_P\}_j - \int_{S_2}\delta f q\,\mathrm{d}S_2 - \sum_{j=1}^{m}\delta\phi_j Q_j = 0,\end{aligned} \tag{34}$$

where F_{s1} are the external forces acting on surface S_1, q is the external charge defined on surface S_2, and Q_j represent the electric concentrated charge at m points.

The element mechanical stiffness matrix resulting from the variational principle reads [33]:

$$\left[\boldsymbol{K}_{uu}\right] = \left[\boldsymbol{K}_{mf}\right] + \left[\boldsymbol{K}_{s}\right] + \left[\boldsymbol{K}_{t}\right] \tag{35}$$

The element stiffness matrix includes membrane-flexural (in plane) [$\boldsymbol{K}_{mf}$], transverse shear [$\boldsymbol{K}_s$] and the so-called torsional (drilling) stiffness [$\boldsymbol{K}_t$]. The former two are easily computed based on the derived strain field:

$$\begin{aligned}\left[\boldsymbol{K}_{mf}\right] &= \int_{Ve}\begin{bmatrix}\left[\boldsymbol{B}_{Tm}\right]^{\mathrm{T}} \\ --- \\ \mathrm{t}\left[\boldsymbol{B}_{R1f}\right]^{\mathrm{T}}\end{bmatrix}\left[\boldsymbol{C}_m\right]\left[\left[\boldsymbol{B}_{Tm}\right] \;\middle|\; t\left[\boldsymbol{B}_{R1f}\right]\right]\mathrm{d}V_{\mathrm{e}} \\ \left[\boldsymbol{K}_{s}\right] &= \int_{Ve}\begin{bmatrix}\left[\boldsymbol{B}_{Ts}\right]^{\mathrm{T}} \\ --- \\ \left[\boldsymbol{B}_{R0s}\right]^{\mathrm{T}} + t\left[\boldsymbol{B}_{R1s}\right]^{\mathrm{T}}\end{bmatrix}\left[\boldsymbol{C}_{\mathrm{s}}\right] \\ &\qquad \left[\left[\boldsymbol{B}_{Ts}\right] \;\middle|\; \left[\boldsymbol{B}_{R0s}\right]^{\mathrm{T}} + t\left[\boldsymbol{B}_{R1s}\right]\right]\mathrm{d}V_{\mathrm{e}}\end{aligned} \tag{36}$$

where [$\boldsymbol{C}_m$] is the part of Hook's matrix relating the in-plane stresses and strains, and [$\boldsymbol{C}_s$] relates the transverse shear stress and strains.

A node has five degrees of freedom in the local coordinate system (two rotations), but as a consequence of transformation there are in general six degrees of freedom in the global coordinate system. This may give rise to numerical problems for a special position of the element leading to zero stiffness for the rotation about one of the global axes. An erratic behavior of the element. A numerically quite simple solution is proposed by Zienkiewicz and Taylor [34] and it implies introduction of additional torsional stiffness. Governing torsional strain energy, E_t, is defined and it serves as a penalty function forcing the local rotation $\theta_{z'}$ to be approximately equal to $0.5(\partial v'/\partial x' - \partial u'/\partial y')$ at integration points:

$$E_t = \frac{1}{2}\alpha_{\mathrm{n}} Y h^n \int_A \left[\theta_{z'} - \frac{1}{2}\left(\frac{\partial v'}{\partial x'} - \frac{\partial u'}{\partial y'}\right)\right]_{(r,s,o)}^2 \mathrm{d}A \tag{37}$$

Here, Y is the Young's elasticity module and α_{n} is a fictitious parameter that can be chosen.

The element dielectric stiffness matrix is given as:

$$\left[\boldsymbol{K}_{\phi\phi}\right] = -\int_V \left[\boldsymbol{B}_{\phi}\right]^{\mathrm{T}}\left[\boldsymbol{d}^{\varepsilon}\right]\left[\boldsymbol{B}_{\phi}\right]\mathrm{d}V \tag{38}$$

It is diagonal as the difference of the electric potentials of one piezoelectric layer affects only the electric field of the very same piezolayer. Analytical integration in the thickness direction yields:

$$\boldsymbol{K}_{\phi\phi} = -\begin{bmatrix} \ddots & & 0 \\ & \dfrac{d'_{33k}}{(h/2)\left(z'_k - z'_{k-1}\right)}\displaystyle\int_{-1}^{+1}\int_{-1}^{+1}\det\left[\boldsymbol{J}_1\right]\mathrm{d}r\mathrm{d}s & \\ 0 & & \ddots \end{bmatrix} \tag{39}$$

where $\boldsymbol{J}_1$ is the Jacobi matrix between the global and natural coordinate system. Given that the boundaries of the element in the parametric space are determined by the parameters ξ and η, mapping from the parametric to the normalized space is also necessary.

$$\det\left[\boldsymbol{J}_{\xi\eta}\right]_k = \frac{\xi_{i+1} - \xi_i}{2} \cdot \frac{\eta_{j+1} - \eta_j}{2} \tag{40}$$

The piezoelectric coupling matrix describes the coupling between the mechanical and the electric field, and it is given as:

$$\left[\boldsymbol{K}_{u\phi}\right] = \left[\boldsymbol{K}_{\phi u}\right]^{\mathrm{T}} = -\int_V \left(\left[\boldsymbol{B}_u\right]^{\mathrm{T}}\left[\boldsymbol{e}\right]^{\mathrm{T}}\left[\boldsymbol{B}_{\phi}\right]\right)\mathrm{d}V \tag{41}$$

7 NUMERICAL EXAMPLE

The considered two examples use a model of a composite cylinder arc with two piezolayers. The structure is a simply supported composite cylindrical arch of the radius R = 100 mm and the width b = 62.8 mm. The composite layers have a "balanced" stacking sequence [45/ − 45/0] s (orthotropic material properties) and the piezolayers, which cover completely the top and bottom surfaces, are oppositely polarized. The thickness of each composite layer is 0.12mm and that of the piezolayers is 0.24 mm. The properties of the composite and piezoelectric layers are given in Tab. 1 [33].

Deformation of the arch is achieved in two different ways with purely mechanical loads and with loads obtained through excitation of the piezolayers by electric voltage.

Although the symmetry of the structure allows to consider its quarter with appropriate boundary conditions applied, it was decided to use the full model as the structure is relatively simple and thus the resulting FE model would not be numerically demanding. The structure is discretized using a NURBS patch with the basis function of degree 4

in arch direction and degree 2 along the cylinder axial direction (width).

Table 1 Material properties

Material properties	PZT G1195 piezolayer	T300/976 graphite/epoxy
Elastic properties		
Y_{11} / GPa	63	150
Y_{22} / GPa	63	9
ν_{12}	0.3	0.3
G_{12} / GPa	24.2	7.1
Piezoelectric properties		
e_{31} (10^{-5} C/mm^2)	2.286	0
e_{32} (10^{-5} C/mm^2)	2.286	0

The mesh has 20 elements and 25 control points in arch direction. Along the cylinder axial direction (width), the number of elements is 4. The obtained results are compared with the results obtained using the classical finite element model discretized with the Reissnerr-Mindlin shell type developed for modeling composite laminates with piezolayers [33]. This is a full biquadratic shell element with 9 nodes. In the case of classical element, three different finite element meshes were used to check the convergence the selected number of elements in the circumferential direction was 10, 20 and 40, respectively.

To check the suitability of the developed FE formulation for both purely mechanical and coupled piezoelectric cases, two different loading cases were considered. The first one is purely mechanical. In this case, the structure is loaded with a vertical force (1N/m) uniformly distributed over the width line that splits the arch into halves. In the second case, the excitation is achieved by means of electric voltage of 100 V supplied to the piezolayers. As the piezolayers have symmetric position with respect to the mid-surface of the arch and are oppositely polarized, this excitation induces bending moments uniformly distributed over the supported edges and the free cylindrical edges of the arch. The presented results of the isogeometric approach indicate excellent agreement with the results reported in previous study (Fig. 6 and Fig. 7), but it should be noted that the isogeometric formulation uses less degrees of freedom to achieve the same accuracy as the classical FE formulation.

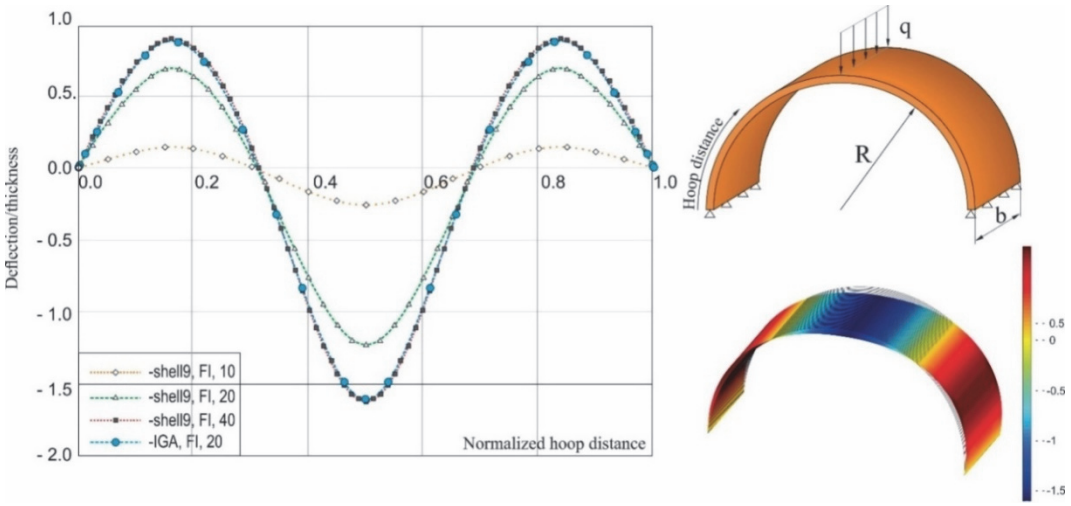

Figure 6 Simply supported composite cylindrical arch under uniformly distributed vertical force

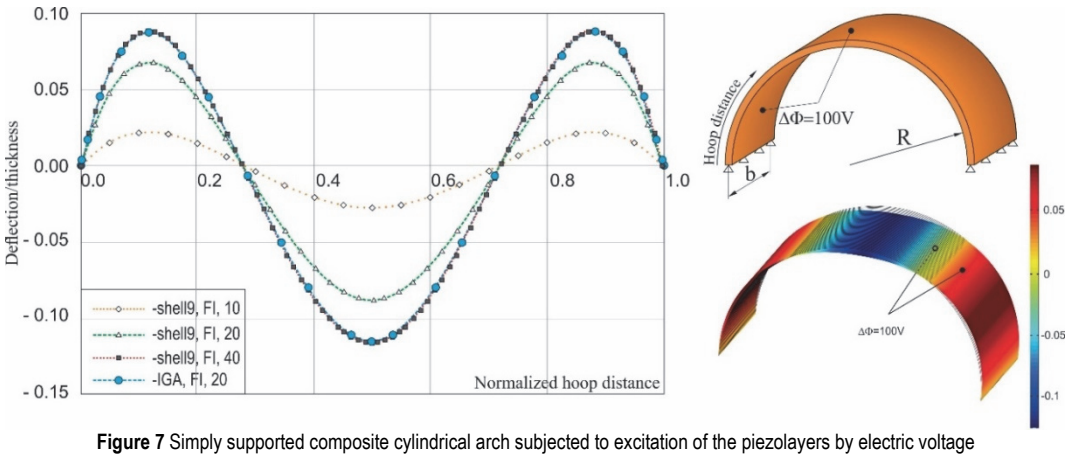

Figure 7 Simply supported composite cylindrical arch subjected to excitation of the piezolayers by electric voltage

8 CONCLUSIONS

Active thin-walled structures have received a great deal of attention over the previous two decades, which is due to the obvious advantages they offer over the classical, passive structures, recognized in the improved dynamical behavior, safety and robustness. Suitable numerical tools that enable their efficient modelling and simulation of their behavior are an important prerequisite for their successful and efficient development.

This paper proposes an isogeometric FE formulation for shell structures made of composite laminates with embedded piezoelectric layers. The piezoelectric layers characterized by the coupled electro-mechanical field may

be used both as actuators and sensors and thus enable active behavior of the considered structures. By coupling sensors to actuators via a controller, adaptive structural behavior is obtained. The developed formulation offers a tool for modeling mechanical and electrical field as well as their coupling in such a structure, and it could be extended in a further step to include a control algorithm and thus test its effects. The formulation covers laminated structures. In order to keep the level of numerical effort in an acceptable realm, the formulation relies on a first-order theory with the Reissner-Mindlin kinematics. Hence, the transverse shear effects are included, which is important for laminated structures made of composite materials, due to their susceptibility to those effects.

The problem of defining a normal to the reference surface was given particular attention. While it is a relatively trivial task in the framework of the classical FE formulations, it turns out to be a relatively cumbersome task in an isogeometric formulation. In this work, the approach based on the Greville's points is adopted.

The structure considered in the example and subjected to both purely mechanical and electrical loading, shows that the developed isogeometric formulation with higher degrees of basic functions offers a good match for the classical FE formulation of a piezolaminated shell. The results are easily matched with less degrees of freedom and therewith with a smaller numerical effort. This is quite promising for further work, which will aim at extension of the formulation for geometrically nonlinear and dynamic analysis.

Acknowledgements

This research was financially supported by the Ministry of Education, Science and Technological Development of the Republic of Serbia (Contract No. 451-03-9/2021-14/200109) and by the Science Fund of the Republic of Serbia (Serbian Science and Diaspora Collaboration Program, Grant No. 6497585).

9 REFERENCES

[1] Hashemi, K. S. H. (2021). Nonlinear vibration response of piezoelectric nanosensor: influences of surface/interface effects. *Facta Universitatis-Series Mechanical Engineering.*

[2] Wang, K., Alaluf, D., Rodrigues, G., & Preumont, A. (2021). Precision Shape Control of Ultra-thin Shells with Strain Actuators. *Journal of Applied and Computational Mechanics*, *7*(Special Issue), 1130-1137. https://doi.org/10.22055/jacm.2020.31899.1987

[3] Todorov, T., Mitrev, R., & Penev, I. (2020). Force analysis and kinematic optimization of a fluid valve driven by shape memory alloys. *Reports in Mechanical Engineering*, *1*(1), 61-76. https://doi.org/10.31181/rme200101061t

[4] Gabbert, U. & Tzou, H. S. (2000). *Smart Structures and Structronic Systems*. Kluwer Academic Publishers, Dordrecht, Boston, Amsterdam.

[5] Shao, S., Song, S., Xu, M., & Jiang, W. (2018). Mechanically reconfigurable reflector for future smart space antenna application. *Smart Materials and Structures*, *27*(9), 095014. https://doi.org/10.1088/1361-665X/aad480

[6] Mitrev, R., Todorov, T., Fursov, A., Fomichev, V., & Il'in, A. (2021). A Case Study of Combined Application of Smart Materials in a Thermal Energy Harvester with Vibrating Action. *Journal of Applied and Computational Mechanics*, *7*(1), 372-381.

[7] Noll, M., Lentz, L., & von Wagner, U. (2019). On the discretization of a bistable cantilever beam with application to energy harvesting. *Facta Universitatis-Series Mechanical Engineering*, *17*(2), 125-139. https://doi.org/10.22190/FUME190301031N

[8] Mohammadkhah, M., Marinkovic, D., Zehn, M., & Checa, S. (2019). A review on computer modeling of bone piezoelectricity and its application to bone adaptation and regeneration. *Bone*, *127*, 544-555. https://doi.org/10.1016/j.bone.2019.07.024

[9] Nguyen, X. & Nguyen, H. (2022). Investigation of influences of fabrication tolerances on operational characteristics of piezo-actuated stick-slip micro-drives. *Facta Universitatis-Series Mechanical Engineering*, *20*(1), 109-126. https://doi.org/10.22190/FUME210311036N

[10] Nestorović, T., Marinković, D., Chandrashekar, G., Marinković, Z., & Trajkov, M. (2012). Implementation of a user defined piezoelectric shell element for analysis of active structures. *Finite Elements in Analysis and Design*, *52*, 11-22. https://doi.org/10.1016/j.finel.2011.11.006

[11] Reddy, J. N. (2003). *Mechanics of Laminated Composite Plates and Shells, Theory and Analysis*. Second Edition. CRC Press. https://doi.org/10.1201/b12409

[12] Gabbert, U., Koppe, H., Seeger, F., et al. (2002). Modelling of smart composite shell structures. *Journal of Theoretical and Applied Mechanics*, *3*(40), 575-593.

[13] Marinkovic, D. & Rama, G. (2017). Co-rotational shell element for numerical analysis of laminated piezoelectric composite structures. *Composites Part B: Engineering*, *125*, 144-156. https://doi.org/10.1016/j.compositesb.2017.05.061

[14] Rama, G., Marinkovic, D. Z., & Zehn, M. W. (2017). Linear shell elements for active piezoelectric laminates. *Smart Structures and Systems*, *20*(6), 729-737.

[15] Kulkarni, S. A. & Bajoria, K. M. (2003). Finite element modeling of smart plates/shells using higher-order shear deformation theory. *Composite Structures*, *62*(1), 41-50. https://doi.org/10.1016/S0263-8223(03)00082-5

[16] Balamurugan, V. & Narayanan, S. (2009). Multilayer higher-order piezolaminated smart composite shell finite element and its application to active vibration control. *Journal of Intelligent Material Systems and Structures*, *20*(4), 425-441. https://doi.org/10.1177/1045389X08095269

[17] Marinković, D., Rama, G., & Zehn, M. (2019). Abaqus implementation of a corotational piezoelectric 3-node shell element with drilling degree of freedom. *Facta Universitatis-Series Mechanical Engineering*, *17*(2), 269-283. https://doi.org/10.22190/FUME190530030M

[18] Rama, G., Marinković, D., & Zehn, M. (2018). Efficient three-node finite shell element for linear and geometrically nonlinear analyses of piezoelectric laminated structures. *Journal of Intelligent Material Systems and Structures*, *29*(3), 345-357. https://doi.org/10.1177/1045389X17705538

[19] Hughes, T. J. R., Cottrell, J. A., & Bazilevs, Y. (2005). Isogeometric analysis: CAD, finite elements, NURBS, exact geometry and mesh refinement. *Computer Methods in Applied Mechanics and Engineering*, *194*(39-41), 4135-4195. https://doi.org/10.1016/j.cma.2004.10.008

[20] Kiendl, J., Bletzinger, K. U., Linhard, J., & Wüchner, R. (2009). Isogeometric shell analysis with Kirchhoff-Love elements. *Computer Methods in Applied Mechanics and Engineering*, *198*(49-52), 3902-3914. https://doi.org/10.1016/j.cma.2009.08.013

[21] Nguyen-Thanha, N., Valizadehb, N., Nguyenc, M. N., Nguyen-Xuand, H., Zhuange, X., Areiasf, P., Zih, G., Bazilevsg, Y., Lorenzisa, De L., & Rabczukb, T. (2015). An extended isogeometric thin shell analysis based on

Kirchhoff-Love theory. *Computer Methods in Applied Mechanics and Engineering*, *284*, 265-291. https://doi.org/10.1016/j.cma.2014.08.025
[22] Milić, P. & Marinković, D. (2015). Isogeometric FE analysis of complex thin-walled structures. *Transactions of FAMENA*, *39*(1), 15-26.
[23] Benson, D. J., Bazilevs, Y., Hsu, M. C., & Hughes, T. J. R. (2010). Isogeometric shell analysis: The Reissner-Mindlin shell. *Computer Methods in Applied Mechanics and Engineering*, *199*(5-8), 276-289. https://doi.org/10.1016/j.cma.2009.05.011
[24] Echter, R., Oesterle, B., & Bischoff, M. (2013). A hierarchic family of isogeometric shell finite elements. *Computer Methods in Applied Mechanics and Engineering*, *254*, 170-180. https://doi.org/10.1016/j.cma.2012.10.018
[25] Yujie, G. & Martin, R. (2015). A layerwise isogeometric approach for NURBS-derived laminate composite shells. *Composite Structures*, *124*, 300-309. https://doi.org/10.1016/j.compstruct.2015.01.012
[26] Hosseini, S., Remmers, J. J., Verhoosel, C. V., & de Borst, R. (2015). Propagation of delamination in composite materials with isogeometric continuum shell elements. *Int. J. Numer. Methods Eng.*, *102*(3), 159-179. https://doi.org/10.1002/nme.4730
[27] Dornisch, W., Klinkel, S., & Simeon, B. (2013). IsogeometricReissner-Mindlin shell analysis with exactly calculated director vectors. *Computer Methods in Applied Mechanics and Engineering*, *253*, 491-504. https://doi.org/10.1016/j.cma.2012.09.010
[28] Adam, C., Bouabdallah, S., Zarroug, M., & Maitournam, H. (2015). Improved numerical integration for locking treatment in isogeometric structural elements. Part II: Plates and shells. *Computer Methods in Applied Mechanics and Engineering*, *284*, 106-137. https://doi.org/10.1016/j.cma.2014.07.020
[29] Piegl, L. & Tiller, W. (1995). *The NURBS Book*. Springer. https://doi.org/10.1007/978-3-642-97385-7
[30] Rogers, D. F. (2001). *An Introduction to NURBS with Historical Perspective*. Academic Press. https://doi.org/10.1016/B978-1-55860-669-2.X5000-3
[31] Gerald, F. (1993). *Curves and surfaces for computer aided geometric design: a practical guide*. 3rd. edition. Academic Press Inc.
[32] Marinković, D., Köppe, H., & Gabbert, U. (2007). Accurate modeling of the electric field within piezoelectric layers for active composite structures. *Journal of Intelligent Material Systems and Structures*, *18*(5), 503-513. https://doi.org/10.1177/1045389X06067139
[33] Marinković, D., Köppe, H., & Gabbert, U. (2006). Numerically efficient finite element formulation for modeling active composite laminates. *Mechanics of Advanced Materials and Structures*, *13*(5), 379-392. https://doi.org/10.1080/15376490600777624
[34] Zienkiewicz, O. C. & Taylor, R. L. (1989). *The finite element method - Volume 1: Basic formulation and linear problems*. McGraw-Hill, New York.

Contact information:

Predrag MILIĆ, PhD, Assistant Professor
University of Niš,
Faculty of Mechanical Engineering in Niš,
Aleksandra Medvedeva 14, 18000 Niš, Serbia
E-mail: predrag.milic@masfak.ni.ac.rsl

Dragan MARINKOVIĆ, PhD, Full Professor
(Corresponding author)
University of Niš,
Faculty of Mechanical Engineering in Niš,
Aleksandra Medvedeva 14, 18000 Niš, Serbia
Lecturer and Research Assistant,
Department of Structural Analysis, Berlin Institute of Technology,
Strasse des 17, Juni 135, 10623 Berlin, Germany
E-mail: dragan.marinkovic@tu-berlin.de

Sandra KLINGE, PhD, Full Professor
Department of Structural Analysis,
Berlin Institute of Technology,
Strasse des 17, Juni 135, 10623 Berlin, Germany
E-mail: sandra.klinge@tu-berlin.de

Žarko ĆOJBAŠIĆ, PhD, Full Professor
University of Niš,
Faculty of Mechanical Engineering in Niš,
Aleksandra Medvedeva 14, 18000 Niš, Serbia
E-mail: zcojba@ni.ac.rs